Homogenization of Thin and Thick Metamaterials and Applications

Abdelwaheb Ourir, Yao Gao, Agnès Maurel, Jean-Jacques Marigo

Chapter 7

Homogenization of Thin and Thick Metamaterials and Applications

Abdelwaheb Ourir, Yao Gao, Agnès Maurel and Jean-Jacques Marigo

Additional information is available at the end of the chapter

http://dx.doi.org/10.5772/66035

Abstract

The wave propagation in structures involving metamaterials can be described owing to homogenization approaches which allow to replace the material structured at the subwavelength scale by an equivalent and simpler, effective medium. In its simplest form, homogenization predicts that the equivalent medium is homogeneous and anisotropic and it is associated to the usual relations of continuity for the electric and magnetic fields at the boundaries of the metamaterial structure. However, such prediction has a range of validity which remains limited to relatively thick devices and it is not adapted to more involved geometries (notably three-dimensional). The following two aspects are considered: (i) we study how the homogenization at the leading order can be improved when the thickness of the device becomes small and (ii) we propose a heuristic extension of the solution given by the leading order homogenization in order to deal with a complex geometry; in the latter case, an application to a demultiplexer device is proposed.

Keywords: metamaterial, homogenization, surface waves, spoof plasmons, guided waves, multiplexing, subwavelength devices

1. Introduction

Metamaterials are artificial materials composed by the periodic arrangement of a unit cell; among the different materials in the unit cell, stratified or layered media involving metallic layers have been extensively studied and throughout this chapter, metallic material is thought in the far infrared, thus in a frequency range where metal behaves as an opaque medium, at the boundaries of which Neumann boundary condition applies. Such metallic arrays enter in the design of metallo-dielectric structures, as the artificial magnetic conductors used in the design of antenna and there is currently renewed interest in such array since they are the key

piece of so-called metasurfaces (with a typical resonant behavior as in the mushroom structure of Sievenpiper [1]). In addition to be able to produce unexpected scattering of electromagnetic waves, these structures can support guided waves and it is for this property that they have been proposed by Pendry et al. [2]. In this context, these guided waves have been called "spoof plasmons" since they mimic, in the far infrared regime, the behavior of plasmons observed in the visible range (plasmons are the wave guided at the flat interface between air and metal and this requires a negative permittivity).

Because of their periodic subwavelength structuration, homogenization approaches are ideal tools to predict within a rigorous mathematical framework the scattering properties of these devices. In this chapter, we will present results coming from homogenization techniques. Our starting point is the simplest homogenization; owing to the small parameter $\eta = kh$, with k the wavenumber and h the typical spacing of the periodic structuration, we call simplest homogenization the homogenization performed at the leading order in η, which is the 0 order. Such homogenization predicts that a stratified medium can be replaced by an equivalent homogeneous and anisotropic medium associated to the usual conditions of continuity of the electromagnetic fields at the boundaries between two media; it has been used for the practical realization of several metamaterial devices, notably in the context of cloaking [3, 4]. Starting from this classical homogenization, which regards the effect of wave propagation in the bulk of the stratified medium, we will focus on two refinements that may be needed to get accurate results: (i) the case of a metallic array of small thickness for which boundary layer effects can become significant or even dominant when compared to the effect of propagation in the bulk; this case requires to conduce the homogenization up to order 1, which does not affect the equation of propagation in the bulk but makes new conditions at the boundaries to appear (these new conditions are called jump conditions), (ii) the case where the metamaterial device is composed of a succession of metallic elements arranged in a three-dimensional geometry. Although homogenization techniques could be used considering the whole device, the resolution may become tricky. Rather, a heuristic extension of the result coming from the classical homogenization is proposed, based on the analysis of the dispersion relations in each part of the whole device.

These two aspects are presented theoretically and the main theoretical results (in terms of the scattering properties or in terms of the dispersion relations of guided waves) are supported by experimental results. As a practical application, the realization of a demultiplexer is proposed, allowing for the frequency selection of an incoming large band signal into different "colored" channels.

2. The starting point: homogenization of metallic arrays at the leading order (order 0)

The present derivation considers first a stratified medium, with the layers made of a transparent media, afterwards the limiting case of metallic arrays in the far infrared is considered (thus, with metallic layers being associated to Neumann boundary conditions at its boundaries). Also, we restrict ourselves to polarized TM waves, for which the transverse magnetic field $H(x)$ ($x = (x_1,x_2)$) is polarized along $\mathbf{e}_3$ and the whole system is invariant by translation along

x_3 (thus, $\partial_{x_3} = 0$). In the harmonic regime, the time dependence of H is $e^{-i\omega t}$ and it is omitted in the following.

For a succession of layers made of transparent media, the wave equation reads

$$\mathrm{div}\left[\frac{1}{\epsilon}\nabla H\right] + k^2 \mu H = 0, \tag{1}$$

with $k = \sqrt{\epsilon_0 \mu_0}\omega$ the wavenumber in the air ((ϵ_0,μ_0) are the permeability and permittivity of the air and ω the frequency). In Eq. (1), (ϵ,μ) denote the relative permeability and permittivity and they are spatially dependent. At each boundary between two layers, the continuities of H and of $1/\epsilon\ \partial_n H$ apply (with ∂_n the normal derivative).

Next, Eq. (1) can be written in an equivalent form, introducing the field $\boldsymbol{C}$

$$\mathrm{div}\,\boldsymbol{C} + k^2 \mu H = 0, \quad \boldsymbol{C} \equiv \frac{1}{\epsilon}\nabla H, \tag{2}$$

with boundary conditions being the continuity of H and of $\boldsymbol{C}.\mathbf{n}$ at the boundaries between two layers (note that the field $\boldsymbol{C}$ is linked to the electric field, see [5]).

2.1. The asymptotic analysis

The idea is to define three regions where different asymptotic expansions will be used, Eq. (3), with respect to the small parameter $\eta = kh$ (with h the periodic spacing of the layers). The inner region contains the boundary between the stratified medium and the air. The two outer regions for $x_1 > 0$ and $x_1 < 0$ are the regions far enough the interface, where the evanescent field can be neglected, while the inner region contains the evanescent field. Next, the inner region and the outer regions are connected using so-called matching conditions, which will constitute the boundary conditions for the outer solutions (see **Figure 1**).

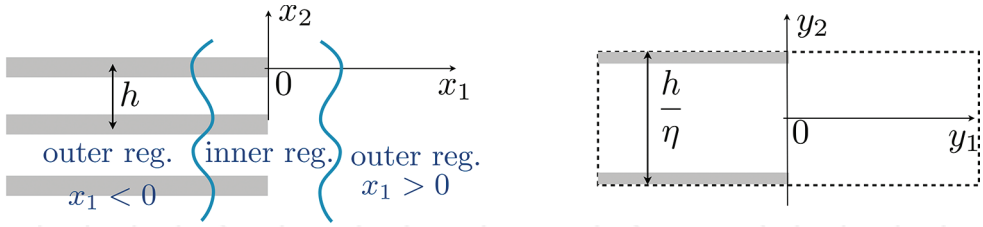

Figure 1. On the left, configuration in the real space with $\mathbf{x} = (x_1,x_2)$ coordinate; the periodicity along x_2 is h; the inner region corresponds to the neighborhood of the boundary between the stratified medium (which occupies the half-space $x_1 < 0$) and the substrate, being the air ($x_1 > 0$). On the right, the unit cell (inner region) in $\mathbf{y} = (y_1,y_2)$ coordinate, with $\mathbf{y} = \mathbf{x}/\eta$. The size of the unit cell along y_2 is h/η with $\eta \equiv kh$.

2.1.1. The outer and inner expansions

The asymptotic expansions are thought with spatial dependences on a *macroscopic* coordinate $\mathbf{x}$ associated with low variations of the fields (with the typical scale $1/k$ of the wave) and a

microscopic coordinate $\mathbf{y}$ associated with rapid variations (with the typical scale h of the layers) and in each region, we keep the coordinates that are relevant to describe the variations of the field. To do so and with $\eta \equiv kh \ll 1$, we define $\mathbf{y} \equiv \mathbf{x}/\eta$ and we assume that (H, $\boldsymbol{C}$) can be expanded by using the following asymptotic expansions

$$\begin{cases} \text{outer region } x_1 > 0, & H = H^0(\mathbf{x}) + \eta H^1(\mathbf{x}) + \ldots, \\ & \boldsymbol{C} = \boldsymbol{C}^0(x) + \eta \boldsymbol{C}^1(\mathbf{x}) + \ldots, \\ \text{outer region } x_1 < 0, & H = H^0(\mathbf{x},y_2) + \eta H^1(\mathbf{x},y_2) + \ldots, \\ & \boldsymbol{C} = \boldsymbol{C}^0(\mathbf{x},y_2) + \eta \boldsymbol{C}^1(\mathbf{x},y_2) + \ldots, \\ \text{inner region}, & H = h^0(x_2,\mathbf{y}) + \eta h^1(x_2,\mathbf{y}) + \ldots, \\ & \boldsymbol{C} = c^0(x_2,\mathbf{y}) + \eta \boldsymbol{c}^1(x_2,\mathbf{y}) + \ldots, \end{cases} \tag{3}$$

with the outer terms (H^n, $\boldsymbol{C}^n$) for $x_1 < 0$ and the inner terms (h^n, $\boldsymbol{c}^n$) being periodic *w.r.t.* y_2. The differential operator reads, in the different regions, as

$$\begin{cases} x_1 > 0, & \nabla \to \nabla_{\mathbf{x}}, \\ x_1 < 0, & \nabla \to \nabla_{\mathbf{x}} + \dfrac{1}{\eta}\dfrac{\partial}{\partial y_2}\mathbf{e}_2, \\ \text{inner region}, & \nabla \to \dfrac{\partial}{\partial x_2}\mathbf{e}_2 + \dfrac{1}{\eta}\nabla_{\mathbf{y}}. \end{cases} \tag{4}$$

2.1.2. The matching conditions

The inner and outer problems have to be associated with boundary conditions or radiation conditions which ensure that the problems are well-posed. Since the outer expansions hold true only far away from the interface, the outer terms do not have to satisfy the continuity conditions at $x_1 = 0$. Reversely, the conditions at infinity satisfied by the inner terms are unknown *a priori*. These missing conditions are provided by the matching conditions, which read at leading order

$$H^0(0^+,x_2) = \lim_{y_1 \to +\infty} h^0(x_2,\mathbf{y}), \tag{5a}$$

$$H^0(0^-,x_2,y_2) = \lim_{y_1 \to -\infty} h^0(x_2,\mathbf{y}), \tag{5b}$$

$$\boldsymbol{C}^0(0^+,x_2) = \lim_{y_1 \to +\infty} \boldsymbol{c}^0(x_2,\mathbf{y}), \tag{5c}$$

$$\boldsymbol{C}^0(0^-,x_2,y_2) = \lim_{y_1 \to -\infty} \boldsymbol{c}^0(x_2,\mathbf{y}). \tag{5d}$$

2.2. The homogenized wave equation at the leading order

We want to establish the wave equation satisfied by the mean fields $\langle H^0 \rangle(x)$ and $\langle \boldsymbol{C}^0 \rangle(x)$ for $x_1 < 0$, where we have defined the average over $y_2 \in Y = (-1/2, 1/2)$. The homogenized wave equation is sought for $x_1 < 0$, only. For $x_1 > 0$, the wave equation is obviously

$$\mathrm{div}_{\mathbf{x}}\boldsymbol{C}^0 + H^0 = 0, \quad \boldsymbol{C}^0 = \nabla_{\mathbf{x}} H^0, \quad \text{for } x_1 > 0, \tag{6}$$

being the same at each order and the fields equal their averages. Eq. (2), at leading order $(1/\eta)$, read $\partial_{y_2}\boldsymbol{C}_2^0 = 0 = \partial_{y_2}H^0$, whence

$$\langle H^0\rangle(\mathbf{x}) = H^0(\mathbf{x}), \quad \langle \boldsymbol{C}_2^0\rangle(\mathbf{x}) = C_2^0(\mathbf{x}). \tag{7}$$

Now, we establish the relation between $\langle \mathbf{C}^0\rangle$ and H^0 (this latter being equal to its average). Eq. (2) at order η^0 in the outer problems $x_1 < 0$ give

$$\boldsymbol{C}^0(\mathbf{x},y_2) = \frac{1}{\epsilon(y_2)}\left[\nabla_{\mathbf{x}}H^0(x) + \frac{\partial H^1}{\partial y_2}(\mathbf{x},y_2)\mathbf{e}_2\right], \tag{8}$$

and

$$\mathrm{div}_{\mathbf{x}}\boldsymbol{C}^0(\mathbf{x},y_2) + \frac{\partial C_2^1}{\partial y_2}(\mathbf{x},y_2) + \mu(y_2)H^0(\mathbf{x}) = 0. \tag{9}$$

Averaging both equations, with $C^0(\mathbf{x},y_2) = C_1^0(\mathbf{x},y_2)\mathbf{e}_1 + C_2^0(\mathbf{x})\mathbf{e}_2$ and owing to the periodicity of H^1 and of C_2^1 w.r.t. y_2 (thus, $\langle\partial_{y_2}H^1\rangle = 0 = \langle\partial_{y_2}C_2^1\rangle$), we easily get the homogenized wave equation at the first order

$$\begin{cases} \langle C^0\rangle(\mathbf{x}) = \left\langle\frac{1}{\epsilon}\right\rangle\frac{\partial H^0}{\partial x_1}(\mathbf{x})\mathbf{e}_1 + \langle\epsilon\rangle^{-1}\frac{\partial H^0}{\partial x_2}(\mathbf{x})\mathbf{e}_2, \\ \mathrm{div}_{\mathbf{x}}\langle\mathbf{C}^0\rangle + \langle\mu\rangle H^0 = 0. \end{cases} \tag{10}$$

2.3. The continuity relations at the leading order

To the homogenized wave equation (10), we have to associate continuity (or discontinuity) conditions at the interface $x_1 = 0$. To that aim, we have to consider the inner solution and its matching with the two outer solutions. We are looking for the quantities $[\![H^0]\!]$ and $[\![\langle C_1^0\rangle]\!]$. Eq. (2) for the inner problem tell us, at the leading order (in $1/\eta$), that $\nabla_{\mathbf{y}}h^0 = 0$ from which h^0 does not depend on $\mathbf{y}$. From the previous section, we already know that $H^0(\mathbf{x})$ does not depend on y_2, from which the matching conditions, Eqs. (5a) and (5b), give

$$H^0(0^+,x_2) = H^0(0^-,x_2) = h^0(x_2), \quad \text{and } [\![H^0]\!] = 0. \tag{11}$$

Next, Eq. (2) in the inner region gives also, at the leading order, $\mathrm{div}_{\mathbf{y}}c^0 = 0$; by integrating this equation on $Y \times]-\infty, +\infty[$, we get

$$\int_Y dy_2[c_1^0(x_2,+\infty,y_2) - c_1^0(x_2,-\infty,y_2)] = 0, \tag{12}$$

(we have used the periodicity of $\boldsymbol{c}^0$ w.r.t. y_2). From the matching conditions Eqs. (5c) and (5d) integrated over Y, we get

$$C_1^0(0^+,x_2) = \langle C_1^0 \rangle\,(0^-,x_2), \quad \text{and } [\![\langle C_1^0 \rangle]\!] = 0. \tag{13}$$

At the first order, the usual continuities of the electromagnetic fields are found.

2.4. The homogenized problem for metallic layers in the far infra red

For rigid layers in the air and denoting φ the filling fraction of air within the stratified medium, we have: in the air $\epsilon = 1 = \mu$; the metal in the far infrared regime can be considered as an opaque medium at the boundaries of which Neumann boundary condition applies; this is correctly accounted for by considering the limiting values $1/\epsilon = 0 = \mu$ (see e.g., [6]). Thus, the homogenized problem reads

$$\boxed{\begin{array}{l}\text{Homogenization at order 0}\\ \begin{cases} \text{div}\boldsymbol{C} + k^2\varphi H = 0, \quad \boldsymbol{C} = \begin{pmatrix} \varphi & 0 \\ 0 & 0 \end{pmatrix} \nabla H, \\ H \text{ and } \boldsymbol{C}.\mathbf{n} \text{ continuous at the boundary of the metallic array.} \end{cases}\end{array}} \tag{14}$$

It is worth noting that the above continuity relation means notably that (i) at the interface with the air, $\varphi \nabla H.\mathbf{n}_{|\text{array}} = \nabla H.\mathbf{n}_{|\text{air}}$ while (ii) at the boundary with a ground plane, the usual Neumann boundary condition applies $\nabla H.\mathbf{n}_{|\text{array}} = 0$.

3. Weakness of the first-order homogenization for small thickness devices

In this section, we inspect the validity of the homogenized problem, Eq. (14). This is done in the configuration of **Figure 2**, where a metallic array is placed in the air and illuminated by a plane wave at oblique incidence θ. We measured experimentally the transmission coefficient T^{exp} for the array of thickness e (and the array structuration is characterized by φ and h) and compared T^{exp} to the transmission coefficient T obtained in the homogenized problem. To anticipate, we

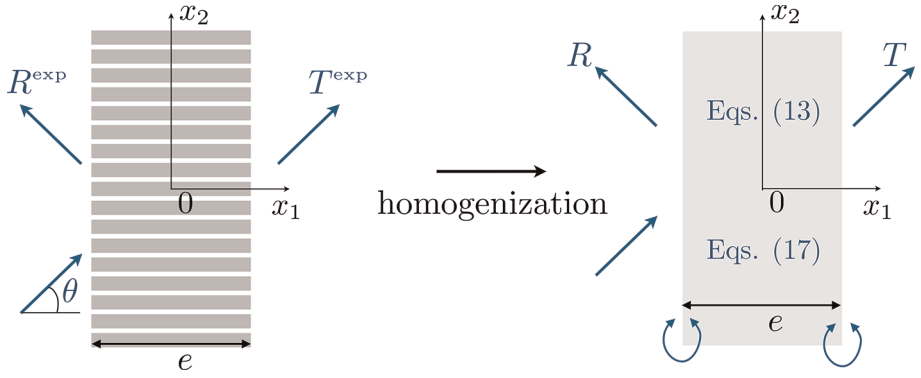

Figure 2. Scattering of an incident plane wave on a slab of stratified medium (the layers are metallic); the homogenization process produces an equivalent slab, described by Eqs. (14) and (18) at order 0 and at order 1, respectively.

http://dx.doi.org/10.5772/66035

shall see that the leading order homogenization may become unsatisfactory for small thicknesses of the array and going up to the homogenization at order 1 is necessary. Thus, the derivation of the scattering coefficients in these homogenized problems is presented first, afterwards comparisons with those measured experimentally are presented.

3.1. The scattering coefficients in the homogenized problems

Let us start with the first-order homogenization, for which the explicit solution of Eq. (14) read

$$\begin{cases} x_1 < -e/2, & H(\mathbf{x}) = \left[e^{ik\cos\ \theta(x_1+e/2)} + Re^{-ik\cos\ \theta(x_1+e/2)}\right]e^{ik\sin\theta x_2}, \\ |x_1| < e/2, & H(\mathbf{x}) = \left[ae^{ikx_1} + be^{-ikx_1}\right]e^{ik\sin\theta x_2}, \\ x_1 > e/2, & H(\mathbf{x}) = Te^{ik\cos\ \theta(x_1-e/2)+ik\sin\theta x_2}. \end{cases} \tag{15}$$

We used the dispersion relations coming from the wave equations $\Delta H + k^2 H = 0$ in the air and $\partial^2_{x_1^2} H + k^2 H$ in the homogenized stratified slab. Next, applying the relations of continuity applying at $x_1 = \pm e/2$, we get the scattering coefficients

$$\begin{cases} R = -\dfrac{z_1 z_2^* e^{ike} - z_1 z_2 e^{-ike}}{z_1^2 e^{ike} - z_2^2 e^{-ike}}, \\ T = \dfrac{|z_1|^2 - |z_2|^2}{z_1^{*2} e^{ike} - z_2^2 e^{-ike}}, \end{cases} \tag{16}$$

where z_i^* denotes the complex conjugate of z_i, $i = 1, 2$. In fact, for the leading order homogenization, (z_1, z_2) are real with

$$z_1 \equiv \left(1 - \frac{\cos\theta}{\varphi}\right), \quad z_2 \equiv \left(1 + \frac{\cos\theta}{\varphi}\right), \tag{17}$$

and $\cos\theta/\varphi$ is the effective impedance mismatch between the two media. As previously said, the leading order homogenization will fail and the next order homogenization is required. This homogenization at order 1 has been considered in [7] and it has been shown that the same equation in the bulk (see Eq. (14)) is obtained, but instead of the continuities of H and $\boldsymbol{C}.\mathbf{n}$ as boundaries conditions, jump conditions are obtained. Specifically, the homogenization at order 1 read

Homogenization at order 1

$$\begin{cases} \mathrm{div}\boldsymbol{C} + k^2\varphi H = 0, \quad C = \begin{pmatrix} \varphi & 0 \\ 0 & 0 \end{pmatrix}\nabla H, \\ [\![H]\!] = \dfrac{h\mathcal{B}}{2}(C^- + \boldsymbol{C}^+).\mathbf{n} \text{ and } [\![\boldsymbol{C}]\!].\mathbf{n} = \dfrac{h\mathcal{C}}{2}\left(\dfrac{\partial^2 H^-}{\partial x_2^2} + \dfrac{\partial^2 H^+}{\partial x_2^2}\right). \end{cases} \tag{18}$$

In the above equations, it appears that both H and $\boldsymbol{C}.\mathbf{n}$ are now discontinuous (the obtained conditions are jump conditions at the boundaries of the stratified medium). This is why $H^{\pm}$ (same for $\boldsymbol{C}$) are defined, as the limit values of H at the boundary. In this case, the expressions of (R, T) in Eq. (16) are still valid, but we get

$$\begin{cases} z_1 \equiv \left(1 - \dfrac{\cos\theta}{\varphi}\right) + \mathrm{i}kh\left(\mathcal{B}\cos\theta + \mathcal{C}\dfrac{\sin^2\theta}{\varphi}\right) - (kh)^2\sin^2\theta\dfrac{\mathcal{BC}}{4}\left(1 + \dfrac{\cos\theta}{\varphi}\right), \\ z_2 \equiv \left(1 + \dfrac{\cos\theta}{\varphi}\right) - \mathrm{i}kh\left(\mathcal{B}\cos\theta - \mathcal{C}\dfrac{\sin^2\theta}{\varphi}\right) + (kh)^2\sin^2\theta\dfrac{\mathcal{BC}}{4}\left(1 + \dfrac{\cos\theta}{\varphi}\right). \end{cases} \tag{19}$$

The parameters $\mathcal{B}$ and $\mathcal{C}$, that we could call boundary parameters, depend only on the filling fraction of air in the layered medium and they are given by

$$\mathcal{B} = -\frac{1}{\pi}\log\sin\left(\frac{\pi\varphi}{2}\right), \quad \mathcal{C} \simeq \frac{\pi}{16}\varphi^2. \tag{20}$$

In principle, (H, $\boldsymbol{C}$) in the homogenization at order 0, Eq. (14), approximate the solution of the actual problem up to $O(\eta)$ and (H, $\boldsymbol{C}$) in the homogenization at order 1, Eq. (18), approximate the solution of the actual problem up to $O(\eta^2)$. Thus, we could expect that the difference between both remains incidental. We will see that it is not the case. The reason is that the jump conditions obtained at order 1 encapsulate the effect of the boundary layers at the entrance and at the exit of the stratified slab and these effects may become dominant compared to the effect of the propagation in the bulk of the slab. This is what we inspect below.

3.2. Experimental measurements of the scattering coefficients for varying slab thicknesses e

To test the ability of the leading order homogenization to capture the scattering properties of a metallic array, we realized six arrays of different thicknesses e = 30 μm and 0.25, 1, 4, 14 and 20 mm. Otherwise, h = 6 mm and $\ell = 5$ mm for the six arrays. We performed the measurements of the transmission coefficients T^{exp} using two X-band frequency horn antennas at both extremities of an electromagnetic chamber (**Figure 3**). The arrays were amounted on a plate able to rotate in order to realize varying incidence angles θ (and the incidence wave is polarized in TM polarization).

We start by reporting in **Figure 4** the spectra $|T^{\mathrm{exp}}|^2$ measured for the two arrays of thickness e = 30 μm and e = 20 mm (right panels). For frequencies in the range [8,12] GHz, the thinnest array realizes $ke \in [5; 7.5] \cdot 10^{-3}$ and the thickest array $ke \in [3; 5]$. On the two left panels, the corresponding spectra $|T|^2$ given by Eq. (16) using the leading order homogenization ((z_1, z_2) given by Eq. (17)) and using the homogenization at order 1 ((z_1, z_2) given by Eq. (19)) are reported for comparison. For e = 30 μm, the leading order homogenization predict $|T| \simeq 1$ in the whole ranges of frequencies and incidence angles. This is clearly not the case for $|T|$ given by the homogenization at order 1 and this latter appears to be in good agreement with $|T^{\mathrm{exp}}|$ (we get $|T - T^{\mathrm{exp}}|/|T^{\mathrm{exp}}| \lceil 3\%$ averaged over all f and θ).

For the thicker array, the transmission predicted by the homogenization at order 0 is closer to the measured transmission; in this case, although the spectra obtained using the homogenization at order 1 reproduces better the form of the measured spectra, the relative errors are in both cases about 15% (these highest discrepancies are due to highest relative errors for transmissions close to 0).

http://dx.doi.org/10.5772/66035

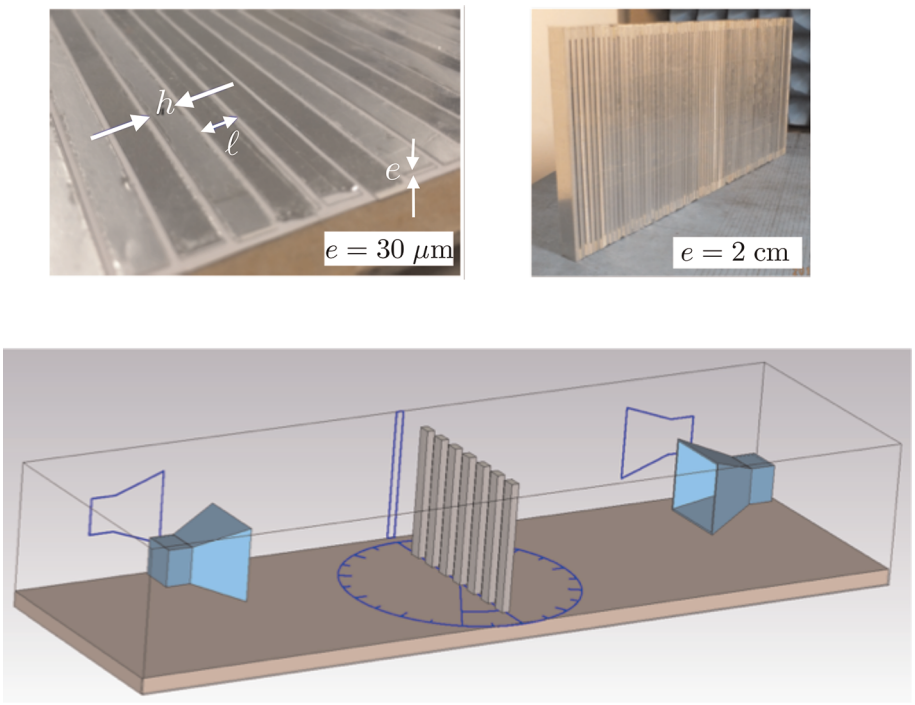

Figure 3. On the top, examples of two metallic arrays; on the bottom, schema of the measurement technique (see text).

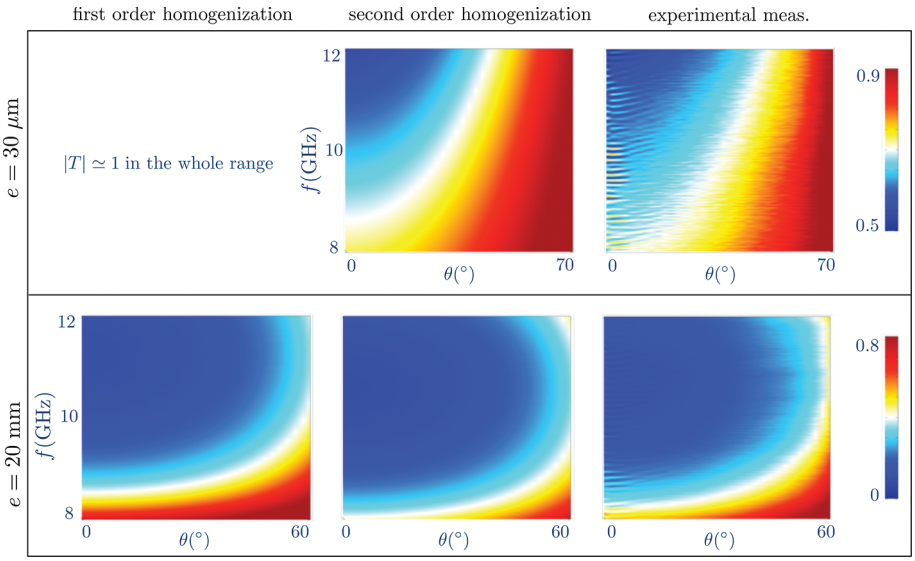

Figure 4. Spectra of transmission as a function of the frequency $f \in [8;12]$ GHz and the incidence angle θ. The left and central panels refer to the results coming from the homogenizations at the order 0 and at the order 1, to be compared with the measured transmission $|T^{\text{exp}}|^2$ (right panel). Spectra are given for the thinner and thicker slabs (see text).

Next, we inspect the variations of the transmission coefficient as a function of ke for the six arrays, **Figure 5**. Each plot corresponds to a fixed frequency (f = 8, 10 and 12 GHz) and we reported $|T^{\text{exp}}|^2$ in blue symbols (each blue point corresponds to one of the six arrays) and $|T|^2$ coming from the homogenization at order 0 (dotted gray lines) and coming from homogenization at order 1 (plain gray lines).

It is visible that thin arrays are not correctly described by the homogenization at order 0. More specifically, it largely underestimates the scattering strength of thin arrays (small e produces systematic large errors in the prediction) and it becomes accurate only when $ke > 1$. To the contrary, the homogenization at order 1 is able to describe the scattering strength of thin and thick arrays.

In conclusion, the homogenization at leading order is valid for $ke < 1$ and $kh < 1$ and thus helpful to predict the behavior of metallic arrays as used in the design of many metamaterial devices (see also [6]). However, care has been taken when using arrays with vanishing thicknesses, typically $ke < 1$. In such cases, the homogenization at order 1 has to be considered. As previously said, this is because the leading order homogenization does not account for the scattering effects of the wave at the entrance and at the exit of the array (these are boundary layer effects) which are correctly accounted for in the homogenization at order 1 through the—boundary—parameters $(\mathcal{B},\mathcal{C})$. For even thinner array, the boundary layer effects at both extremities of the array may interact and another homogenization strategy has to be

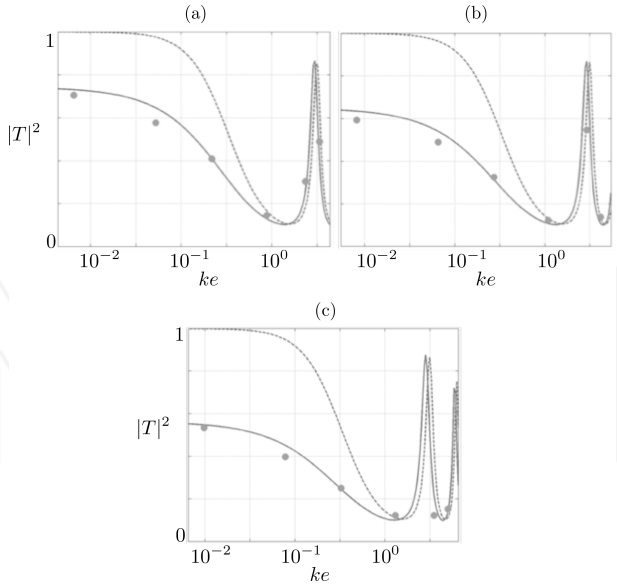

Figure 5. Transmission coefficients as a function of e; $|T^{\text{exp}}|^2$ measured for the six arrays (blue symbols), $|T|^2$ coming from the homogenization at order 0 (dotted gray lines) and coming from the homogenization at order 1 (plain gray lines), (a) $f = 8$ GHz, (b) $f = 10$ GHz and (c) $f = 12$ GHz.

considered; it is called interface homogenization [7] and a practical application of this interface homogenization has been proposed for metallo-dielectric device [5].

4. Use of the results coming for the first-order homogenization for metamaterials with complex geometry

In this section, we investigate another configuration of wave propagation where predictions provided by the homogenization are useful. We consider the ability of periodic structures to present a band structure, with frequency ranges where the wave propagation is forbidden (band gaps) and frequency ranges where the propagation of guided waves is allowed (pass-bands). We study a structure based on such principle. First, the dispersion relation of guided waves within a periodic media (made of metallic plates or metallic rods) is discussed and it is shown that the leading order homogenization is able to reproduce the real dispersion relation. Next, a system of waveguides is thought, based on the band structures of the periodic media, in the waveguide and in the surrounding medium. The application of demultiplexing RF signals is proposed and experimentally validated.

4.1. Dispersion relation of waves guided in a periodic medium

Let us start with the derivation of the wave guided in a 2D stratified medium (the famous "spoof plasmon," **Figure 6a**). In the homogenized problem, Eq. (14), this wave corresponds to the solution of the homogeneous problem (solution in the absence of source), for which the solution reads

$$\begin{cases} 0 < x_1 < e, & H(\mathbf{x}) = \dfrac{\cos kx_1}{\cos ke}\, e^{i\beta x_2}, \\ x_1 > e, & H(\mathbf{x}) = e^{-\sqrt{\beta^2 - k^2}(x_1 - e)}\, e^{i\beta x_2}. \end{cases} \tag{21}$$

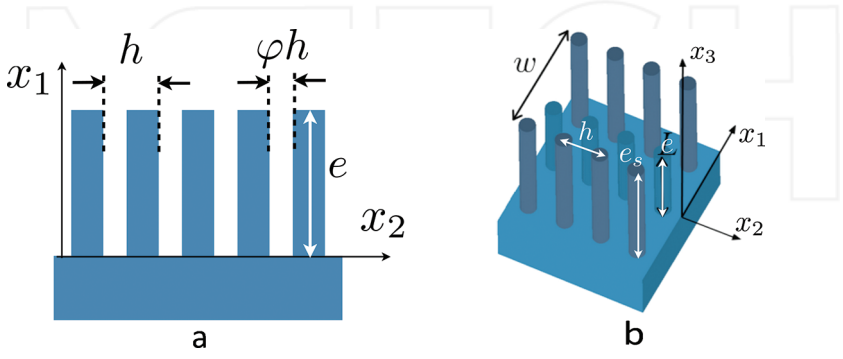

Figure 6. (a) 2D geometry of metallic layers between a ground plane and the air, spoof plasmons can propagate according to Eq. (22), (b) 3D geometry of a structured waveguide of width w, guided modes can propagate according to Eq. (27).

In the above expression, the field H for $0 < x_1 < e$ has been written in order to satisfy the Neumann boundary condition on the ground plane ($\partial_{x_1} H(0,x_2) = 0$) and the continuity of $H(e,x_2)$. It is easy to see that applying the second relation of continuity, namely $\varphi \partial_{x_1} H(e^-,x_2) = \partial_{x_1} H(e^+,x_2)$ coming from Eq. (14), we obtain the dispersion relation of the guided waves

$$\beta^2 = k^2\left[1 + \varphi^2 \tan^2 ke\right], \quad \tan ke > 0, \tag{22}$$

with φ the filling fraction of air and e the length of the layers in the stratified medium. This dispersion relation has been established previously using approximate modal method [2] and it is easily obtained by considering the equivalent homogenized problem.

It is worth noting that such guided wave propagates in the homogenized medium described by the wave equation

$$\frac{\partial^2 H}{\partial x_1^2} + k^2 H = 0, \tag{23}$$

(according to Eq. (14)) and basically, the wave equation (23) tells us that the wave inside the grooves can only propagate along one direction (the x_1-direction). While in principle the upper frequency f_c^+ of the band gap is obtained for $ke = \pi/2$, from Eq. (22), it is in practice limited by the first Brillouin zone $\beta = \pi/h$, whence

$$f_c^+ \sqrt{1 + \varphi^2 \tan^2 \frac{2\pi e f_c^+}{c}} = \frac{c}{2h}, \quad f_c^+ < \frac{c}{4e}. \tag{24}$$

Now, we want to go toward a 3D structuration (**Figure 6b**), where rods are considered, with radius r, periodic spacing h along x_2 and x_3 and height e. The extension of the homogenization results (Eq. (14)) to three dimensions is easy and we find that a periodic structuration of rods produce an equivalent transverse isotropic medium, with the axis of anisotropy along e_1 (the two other directions are equivalent, now φ the volume fraction of air in the rods, whence $\varphi = 1 - \pi r^2/a^2$). Let us consider that these rods forms a waveguide surrounded by a set of higher rods with height e_s (the surrounding rods form the surrounding medium SM) and imagine that we work in a frequency range such that

$$f > \frac{c}{4e_s}, \tag{25}$$

that is in the band gap of the surrounding medium, from which $H \simeq 0$ (for $x_3 < 0$ and $x_3 > w$). Thus, it sounds reasonable to impose $H = 0$ at $x_3 = 0, w$, as boundary conditions for the field in the waveguide with the rods of height e. Looking for the existence of guided wave in the waveguide, we extend the homogenization result to this 3D configuration assuming a solution of the form

$$\begin{cases} 0 < x_1 < e, & H(\mathbf{x}) = \dfrac{\cos kx_1}{\cos ke}\, e^{i\beta x_2}\, \sin\left(\dfrac{\pi x_3}{w}\right), \\ x_1 > e, & H(\mathbf{x}) = e^{-\sqrt{\beta^2 - k^2}(x_1 - e)}\, e^{i\beta x_2}\, \sin\left(\dfrac{\pi x_3}{w}\right). \end{cases} \tag{26}$$

In the simple form thought above, we added heuristically dependence in the x_3 direction which accounts for Dirichlet boundary conditions at $x_3 = 0,w$, when working in the band gap of the surrounding medium.

Otherwise, Eq. (26) accounts for the continuity of H at the interface with the air and for the Neumann boundary condition at the ground plane; as previously, the additional condition $\varphi \partial_z H(L^-) = \partial_z H(L^+)$ yields the new dispersion relation

$$\beta^2 = k^2\left[1 + \varphi^2 \tan^2 ke\right] - \left(\frac{\pi}{w}\right)^2. \tag{27}$$

In Eq. (27), the band gap above f_c^+ still exists and it does not significantly differ from Eq. (24) (it is sufficient to replace $c/(2h)$ in the right-hand side term of Eq. (24) by $c\sqrt{1 + (h/w)^2}/(2h)$); but now, a new band gap has appeared below the cut-off frequency f_c^- (given from Eq. (27) for $k \tan ke = \pi/(w\varphi)$), whence

$$f_c^- \tan \frac{2\pi f_c^-}{c} = \frac{c}{2w\varphi}. \tag{28}$$

The existence of the resulting finite pass band operating in the frequency range $[f_c^-, f_c^+]$ is the key to realize filtering; in the following, we denote

$$\mathrm{FR}(\text{ waveguide}) = [f_c^-, f_c^+]$$

this frequency range and we refer to w_n, with n an integer, a waveguide obtained when n lines of rods have been shortened (with resulting height e) with respect to the rods of height e_s forming the surrounding medium (SM); the w_n waveguide has a width $w = (n + 1)h$.

4.2. Experimental validation of the homogenized dispersion relation

To begin with, we validate experimentally the existence of the pass band and check the validity of our predictions of the FR with bounds f_c^+, f_c^- in Eqs. (24) and (28) and of the associated wavenumbers Eq. (27). Structures containing a waveguide w_1 ($w = 2h$) and a waveguide w_3 ($w = 4h$) have been realized. The surrounding medium is in both cases made of rods with h = 7 mm, r = 3 mm and e_s = 30 mm. The shortened rods have e = 17 mm.

First, we report measurements of the electric field in the range [2.1– 4] GHz (**Figure 7** for w_1). This has been done in a semianechoic chamber using an Agilent 8722ES network analyzer; an *S*-band coaxial-to-waveguide transition has been used as an excitation source and an electric near-field probe mounted on a motorized two-dimensional scanning system has been used to measure the field distribution at a distance of about 1 mm above the structure. The wave

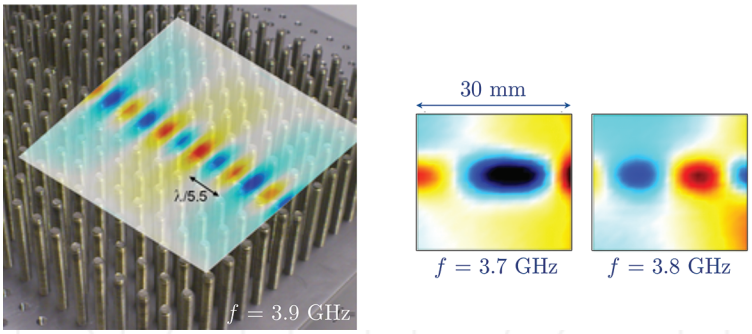

Figure 7. Wavefields of the guided wave in the w_1 waveguide at f = 3.7, 3.8 and 3.9 GHz.

f (GHz)	**3.7**	**3.8**	**3.9**
measured λ_{GW} (mm)	42	30	21
$\lambda_{GW} = 2\pi/\beta$ from Eq. (26)	43	28	20

Table 1. Wavelength λ_{GW} of the guided wave in the w_1 waveguide, measured experimentally and given by Eq. (27).

guided within the waveguide w_1 is visible at f = 3.7, 3.8 and 3.9 GHz, as expected from the frequency range FR(w_1) = [3.6–4] GHz (see **Table 1**).

To go further, we report the transmission in the w_1 and w_3 waveguides as a function of the frequency (**Figure 8**). This has been done by placing a second coaxial-to-waveguide transition at the end of the waveguide and by implementing a normalization to the free air transmission between the emitter and the receptor. In both cases, the existence of a finite pass band is confirmed (the waveguide is called colored) and the observed bounds of the FR are in good agreement with our predictions (the theoretical dispersion relations are reported, with FR(w_3) = [3.1–4]). One can notice here the importance of the attenuation for the spoof-plasmon modes providing the smallest wavelengths. These wavelengths correspond to the highest frequencies in the transmission bands. This phenomenon, known in plasmonics, happens due to intrinsic losses in the considered materials for the high-wave-vector components.

4.3. Application to the design of a demultiplexer

This validation being performed, a multichannel demultiplexer is easy to design; the principle of the demultiplexing is shown in **Figure 5**. A main waveguide, called white guide, is built in order that the FR(white) covers the working frequency range; this is done by choosing: (i) w large enough to produce a small enough f_c^- (see Eq. (28)) and (ii) e small enough to produce a large enough f_c^+ (see Eq. (24)). By setting $w = 10h = 70$ mm and e = 15 mm, we expect FR(white) [2.5–4.5] GHz.

http://dx.doi.org/10.5772/66035

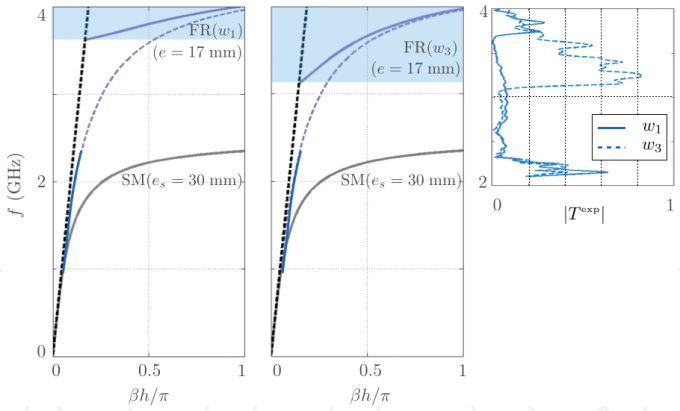

Figure 8. Theoretical dispersion relations of the guided wave in the w_1 (left panel) and w_3 (center panel), given by the plain blue curves, given by Eq. (27). The dispersion relation of the surrounding medium is indicated in plain gray lines, defining a band gap for $f > 2.35$ GHz. Dotted blue lines show the usual dispersion relations of spoof plasmons, Eq. (22), for the periodic array of rods alone (with $e = 17$ mm). Right panel: experimental measurement of the transmission for the w_1 and w_3 waveguides in the range [2.1–4] GHz.

Next, three-colored waveguides (red, green and blue) are thought in order to support guided mode propagation in three different frequency ranges with no overlapping (see **Figure 9**). Again from Eqs. (23) and (27), thin FR are obtained for small w and we set $w = 2h = 14$ mm. By choosing $L = 17$, 19 and 21 mm, we expect this condition to be fulfilled with

$$\begin{cases} \text{FR(red)} = [3 - 3.3] \quad \text{FR(green)} = [3.3 - 3.6] \\ \text{FR(blue)} = [3.6 - 4.0]. \end{cases} \tag{29}$$

The efficiency of the demultiplexer has been tested experimentally and it is illustrated in **Figure 10**. The frequency selection of the colored channel are visible, with the red channel

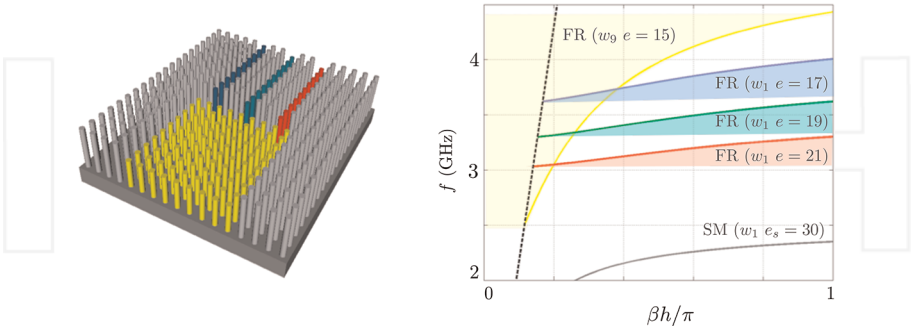

Figure 9. (a) Design of the demultiplexer, the large channel supports guided waves in the whole working frequency range [2.5–4.5] GHz, while each colored channel supports guided waves in a limited frequency range, with no overlapping of the three ranges. (b) Corresponding dispersion relations given by the homogenization, Eq. (27). The gray line shows the dispersion relation of the surrounding medium (all channels work in the band gap of the surrounding medium); the dotted black line shows the light line.

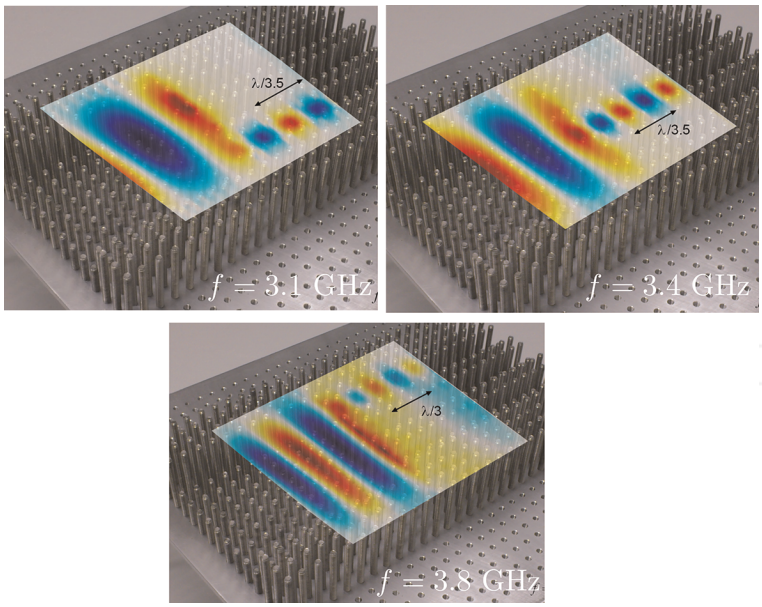

Figure 10. Electric fields scanned above the structure at 3 frequencies chosen respectively in the red (f = 3.1 GHz), in the green (f = 3.4 GHz) and in the blue (f = 3.8 GHz) frequency range $[f_{c-};f_{c+}]$.

being active for $f = 3.1$ GHz, the green channel for $f = 3.4$ GHz and the blue channel for $f = 3.8$. Also as expected, the white channel is active for the three considered frequencies.

5. Conclusion

The design of devices made of subwavelength periodic structure can be helped using the various theoretical predictions provided by homogenization approaches. Among the different homogenization technique, the one presented in this chapter has the advantage to be developed within a rigorous mathematical framework and it yields predictions in a deductive way, that is without any adjustable parameters. We illustrate the ability of such techniques for the scattering properties of metamaterial devices (underlying the limit of the simplest homogenization) and for the ability of certain metamaterial devices to support guided waves of "spoof plasmon" type.

As indicated throughout this chapter, alternative forms of homogenizations can be used, which are more adapted to thin devices. These theoretical tools can be used in order to realize the control of light propagation in a desired way.

Author details

Abdelwaheb Ourir[1]*, Yao Gao[1], Agnès Maurel[1] and Jean-Jacques Marigo[2]

*Address all correspondence to: a.ourir@espci.fr

1 Institut Langevin, CNRS, ESPCI, Paris, France

2 Solid Mechanics Laboratory, CNRS, Polytechnic Institute, Palaiseau, Paris, France

References

[1] D. F. Sievenpiper, High-impedance electromagnetic surfaces, Ph.D. thesis, University of California, Los Angeles (1999).

[2] J. B. Pendry, L. Martn-Moreno, F. J. Garcia-Vidal, Mimicking surface plasmons with structured surfaces, Science. 305 (5685) (2004) 847–848. arXiv:http://www.sciencemag.org/content/305/5685/847.full.pdf, doi:10.1126/science.1098999. URL http://www.sciencemag.org/content/305/5685/847.abstract

[3] M. Farhat, S. Guenneau, S. Enoch, Ultrabroadband elastic cloaking in thin plates, Phys. Rev. Lett. 103 (2009) 024301. doi:10.1103/PhysRevLett.103.024301. URL http://link.aps.org/doi/10.1103/PhysRevLett.103.024301

[4] C. P. Berraquero, A. Maurel, P. Petitjeans, V. Pagneux, Experimental realization of a water-wave metamaterial shifter, Phys. Rev. E. 88 (2013) 051002. doi:10.1103/PhysRevE.88.051002. URL http://link.aps.org/doi/10.1103/PhysRevE.88.051002

[5] A. Maurel, J. J. Marigo, A. Ourir, Homogenization of ultrathin metallo-dielectric structures leading to transmission conditions at an equivalent interface, J. Opt. Soc. Am. B. 33 (5) (2016) 947–956. doi:10.1364/JOSAB.33.000947. URL http://josab.osa.org/abstract.cfm?URI=josab-33-5-947

[6] J. F. Mercier, M. L. Cordero, S. Félix, A. Ourir, A. Maurel, Classical homogenization to analyse the dispersion relations of spoof plasmons with geometrical and compositional effects, Proceedings of the Royal Society of London A: Mathematical, Physical and Engineering Sciences 471 (2182). arXiv:http://rspa.royalsocietypublishing.org/content/471/2182/20150472.full.pdf, doi:10.1098/rspa.2015.0472. URL http://rspa.royalsocietypublishing.org/content/471/2182/20150472

[7] J. J. Marigo, A. Maurel, Homogenization models for thin rigid structured surfaces and films, J. Acoust. Soc. Am. 140 (1) (2016) 260–273. doi:http://dx.doi.org/10.1121/1.4954756. URL http://scitation.aip.org/content/asa/journal/jasa/140/1/10.1121/1.4954756